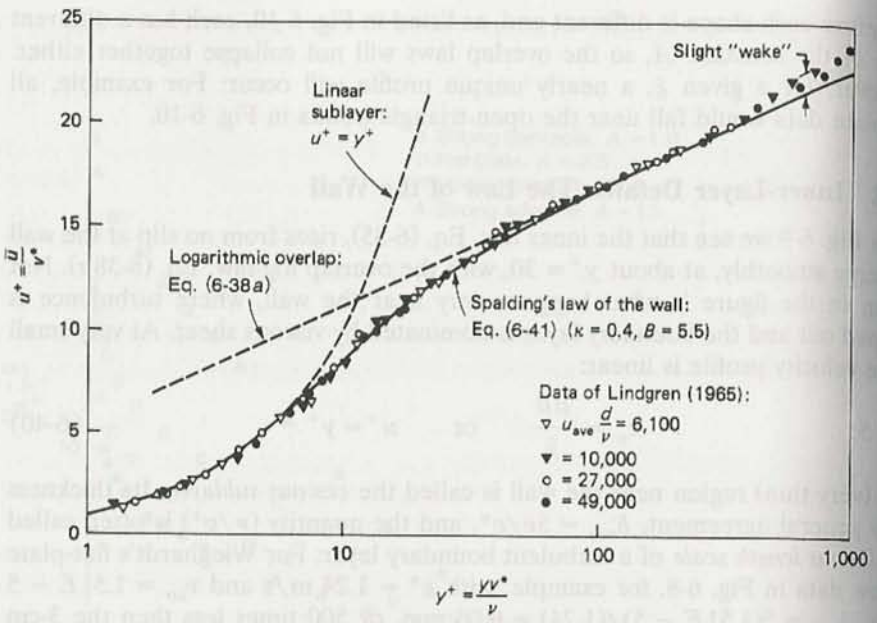

FIGURE 6-11
Comparison of Spalding's inner-law expression with the pipe-flow data of Lindgren (1965).

sensitive to the pressure gradient parameter $\xi = (\delta/\tau_w)(dp_e/dx)$ and its variation with x, as shown by Eq. (6-36) or Fig. 6-10.

In two classic papers, Clauser (1954, 1956) developed the idea of specific cases, for which ξ is constant, which he termed *equilibrium turbulent flows*. Clauser replaced the fuzzily defined thickness δ by the rigorously defined displacement thickness, so that the equilibrium pressure gradient parameter is now taken to be

$$\beta = \frac{\delta^*}{\tau_w}\frac{dp_e}{dx} \qquad \text{Clauser's equilibrium parameter} \tag{6-42}$$

it turns out that constant-β flows correspond to a power-law freestream distribution $U_e = (\text{const})x^m$, exactly analogous to the laminar Falkner-Skan similarity flows of Sec. 4-3.4.

With considerable experimental effort, Clauser (1954) showed clearly that a boundary layer with variable $p_e(x)$ but constant β is in turbulent equilibrium in the sense that all the gross properties of that boundary layer can be scaled with a single parameter. The most relevant thickness parameter for equilibrium flow was determined by Clauser to be the *defect thickness* Δ

$$\Delta = \int_0^\infty \frac{U_e - \bar{u}}{u^*}\,dy = \delta^*\lambda \tag{6-43}$$

where $\lambda = \sqrt{2/C_f}$ is a measure of the local skin friction (λ will be very useful

in some approximate analyses which follow). Velocity profiles could be scaled with y/Δ, and a shape factor G which would remain constant in an equilibrium boundary layer was also defined by Clauser

$$G = \frac{1}{\Delta}\int_0^\infty \left(\frac{U_e - \bar{u}}{u^*}\right)^2 dy \tag{6-44}$$

The ordinary Kármán-type shape factor, $H = \delta^*/\theta$, can be related to G as follows:

$$H = \left(1 - \frac{G}{\lambda}\right)^{-1} \tag{6-45}$$

Since the skin friction varies with x, it follows that H is *not* constant in an equilibrium boundary layer.

There is no longer any doubt about the validity of Clauser's outer-layer structural assumptions. Figure 6-12 shows the outer-layer defect profile for the flat plate ($\beta = 0$), including data for rough walls. The data collapse beautifully about the eddy viscosity calculations of Mellor and Gibson. Also shown are the two equilibrium adverse gradients generated in the original experiments by Clauser (1954), again with excellent agreement. The two distributions are now commonly called Clauser I ($\beta \approx 1.8$, $G \approx 10.1$) and Clauser II ($\beta \approx 8.0$, $G \approx 19.3$). The equilibrium concept is even valid at the ultimate limit ($\beta \to \infty$) as measured, for example, by Stratford (1959). Also, the case of negative β (favorable gradient) is in equally good agreement with experiment, as shown by Herring and Norbury (1967), for example.

6-4.4 An Alternate View: Coles' Law of the Wake

From an application point of view, there are two difficulties with the outer-layer approach of Clauser: (1) nonequilibrium flows deviate in shape from the "similarity" profiles of Fig. 6-12 and (2) even the equilibrium shapes have no simple analytical form to use in an engineering theory. These points were resolved by Coles (1956), who noted that the *deviations* or excess velocity of the outer layer above the log layer (see Fig. 6-9) have a wakelike shape when viewed from the freestream. If normalized by the maximum deviation at $y = \delta$, the data nearly collapse into a unique function of y/δ. In other words, Coles proposed that

$$\frac{u^+ - u^+_{\text{log-law}}}{U_e^+ - u^+_{\text{log-law}}(y = \delta)} \approx f\left(\frac{y}{\delta}\right)$$

where the *wake function* f is normalized to be zero at the wall and unity at $y = \delta$. Two popular curve fits are used for the S shape we expect for the wake function:

$$f(\eta) \approx \sin^2\left(\frac{\pi}{2}\eta\right) \approx 3\eta^2 - 2\eta^3 \tag{6-46}$$

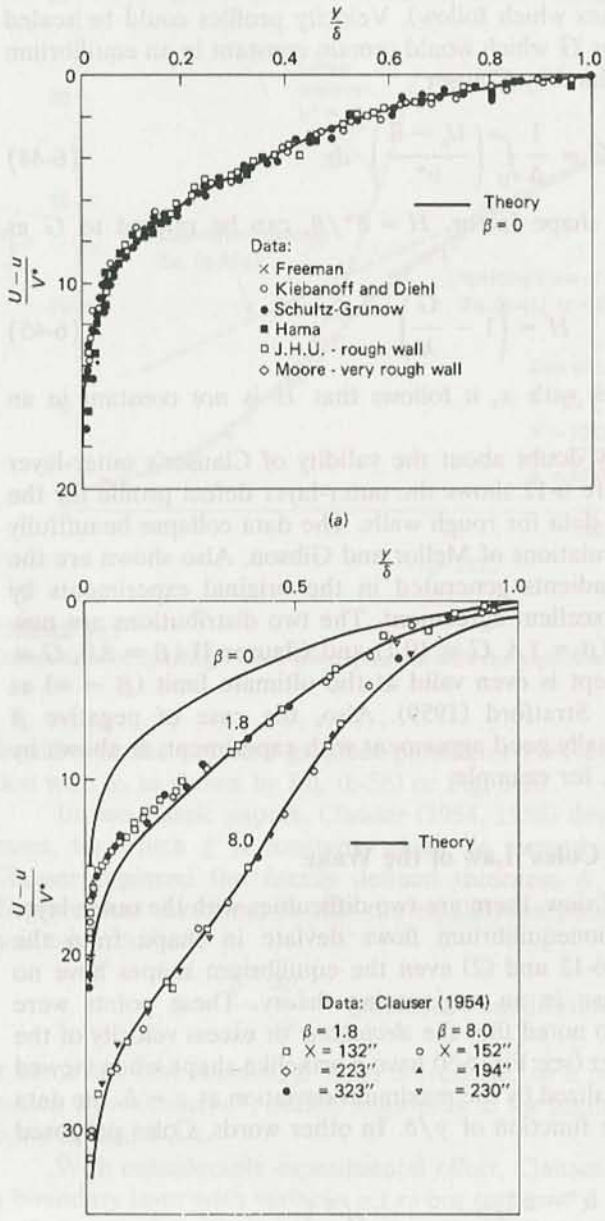

FIGURE 6-12
Equilibrium-defect profiles as correlated by the Clauser parameter β and the theory of Mellor and Gibson (1966): (*a*) flat-plate data; (*b*) equilibrium adverse gradients.

The polynomial fit is easier to use in integral theories.

By adding the wake to the log-law, we have an accurate approximation to both the overlap and outer layers:

$$u^+ \approx \frac{1}{\kappa} \ln(y^+) + B + \frac{2\Pi}{\kappa} f\left(\frac{y}{\delta}\right) \tag{6-47}$$

The quantity Π, called *Coles wake parameter*, is directly related to the previously defined outer-variable constant A, $\Pi = \kappa A/2$. It is also approximately related to Clauser's equilibrium parameter β (see Fig. 6-27). For equilibrium flows, Π should vary only with β.

The beauty of Eq. (6-47) is that it is a complete and reasonably accurate expression for any two-dimensional turbulent-boundary-layer profile, whether in equilibrium or not. If $y^+ < 30$, one should omit the wake and compute u^+ from Eq. (6-41). The efficacy of Eq. (6-47) is seen from the representative profiles plotted in Fig. 6-13, demonstrating the idea of adding an S-shaped wake function to the pure law of the wall ($\Pi = 0$). These are very realistic shapes and easy to compute. If normalized to u/U_e and replotted, they closely resemble the profiles shown in Fig. 6-8.

The wall-wake composite profile can be used in several types of turbulent shear-flow theories. Its admirable simplicity, for example, results in concise

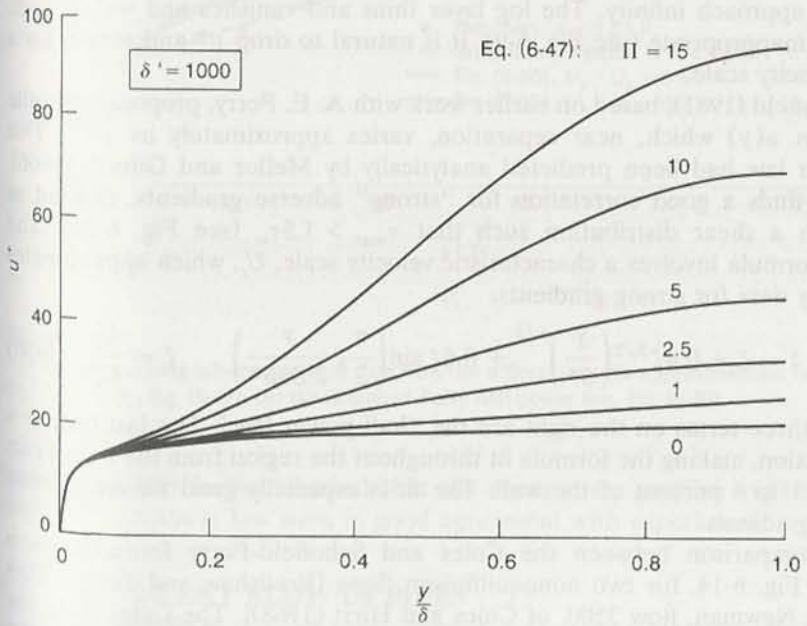

FIGURE 6-13
Turbulent velocity profiles computed from the Coles wall-wake formula, Eq. (6-47), assuming $\delta^+ = 1000$. The curve for $\Pi = 0$ is the pure law of the wall from Eq. (6-41).

formulas for integral parameters. By integrating Eq. (6-47) across the boundary layer, we obtain

$$\frac{\delta^*}{\delta} \approx \frac{1+\Pi}{\kappa\lambda} \qquad \lambda = \left(\frac{2}{C_f}\right)^{1/2}$$
$$\frac{\theta}{\delta} \approx \frac{\delta^*}{\delta} - \frac{2 + 3.2\Pi + 1.5\Pi^2}{\kappa^2\lambda^2} \tag{6-48}$$

Similarly, the local skin-friction coefficient, $C_f = 2\tau_w/\rho U_e^2$, may be related to Π and local Reynolds number, $Re_\delta = U_e\delta/\nu$, by evaluating the wall-wake law (6-47) at the edge of the boundary layer:

$$\frac{U_e}{v^*} = \lambda = \left(\frac{2}{C_f}\right)^{1/2} = \frac{1}{\kappa}\ln\left(\frac{Re_\delta}{\lambda}\right) + B + \frac{2\Pi}{\kappa} \tag{6-49}$$

We will use this simple algebraic approach for some practical turbulent shear-flow problems in the next sections.

6-4.5 Strong Pressure Gradients: The Half-Power Law

As an adverse pressure gradient increases indefinitely, v^* approaches zero and Π and β approach infinity. The log layer thins and vanishes and wall coordinates are inappropriate (see Fig. 6-9). It is natural to drop v^* and search for a better velocity scale.

Schofield (1981), based on earlier work with A. E. Perry, proposes a profile correlation $u(y)$ which, near separation, varies approximately as $y^{1/2}$. This half-power law had been predicted analytically by Mellor and Gibson (1966). Schofield finds a good correlation for "strong" adverse gradients, defined as flows with a shear distribution such that $\tau_{max} > 1.5\tau_w$ (see Fig. 6-24). The curve-fit formula involves a characteristic velocity scale, U_s, which approximates all velocity data for strong gradients:

$$\frac{\bar{u}}{U_\infty} \approx 1 - \zeta + 0.4\zeta^{3/2}\left(\frac{y}{\delta^*}\right)^{1/2} + 0.6\zeta\sin\left(\frac{\pi}{2}\zeta\frac{y}{2.86\delta^*}\right) \qquad \zeta = \frac{U_s}{U_\infty} \tag{6-50}$$

The first three terms on the right are the "half-power law." The last term is a wake function, making the formula fit throughout the region from the freestream to within 1 to 4 percent of the wall. The fit is especially good for equilibrium pressure gradients.

A comparison between the Coles and Schofield-Perry formulations is shown in Fig. 6-14, for two nonequilibrium flows [Bradshaw and Ferriss, flow 2400, and Newman, flow 3500, of Coles and Hirst (1968)]. The Coles wake law (6-47) is reasonably accurate in Fig. 6-14*a*, the chief discrepancy being the difficulty of defining δ accurately. The Schofield-Perry law (6-50) fits well in the intermediate region if the appropriate value of (U_e/U_s) is found. The outer profile is then fit very well if the sine function is added from Eq. (6-50).

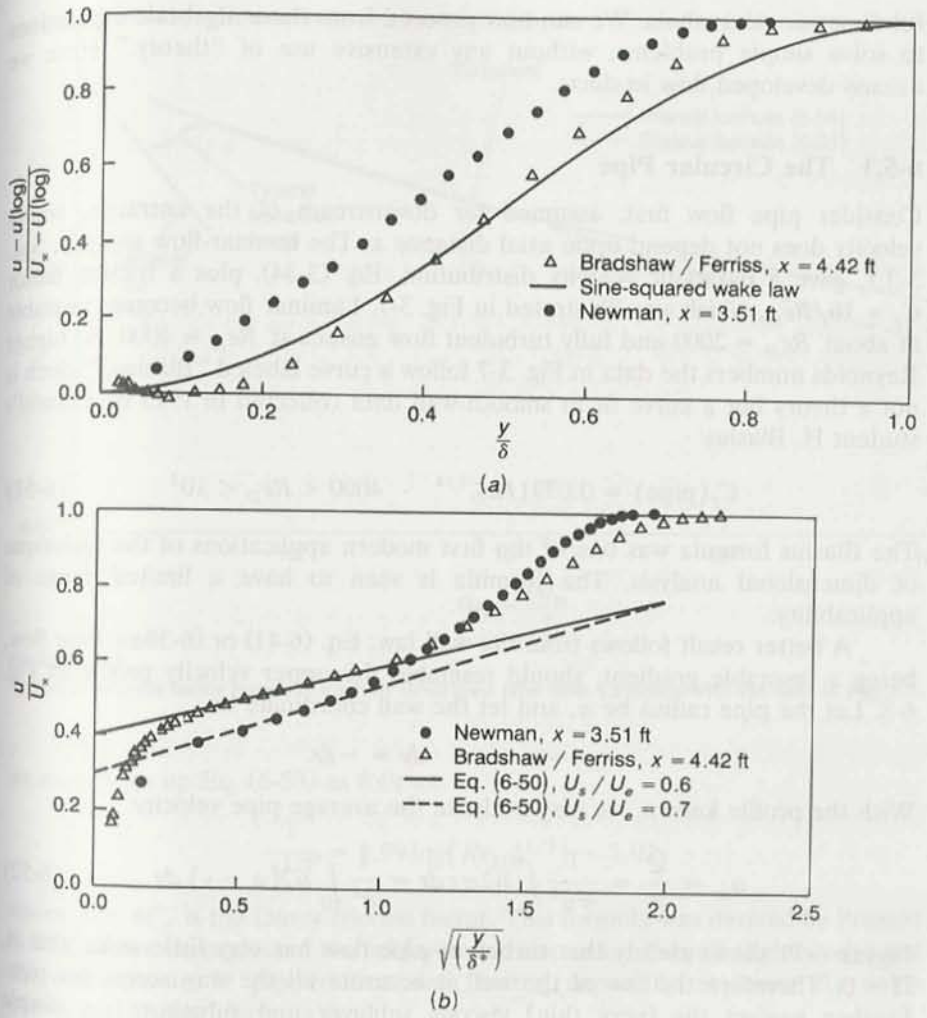

FIGURE 6-14
Comparison of strong adverse gradient data with two different profile approximations: (*a*) the Coles law of the wake, Eq. (6-47); (*b*) the Schofield-Perry half-power law, Eq. (6-50).

Schofield (1981) further showed that the shear-stress profiles $\tau(y)$ computed from the half-power law were in good agreement with experiment.

6-5 TURBULENT FLOW IN PIPES AND CHANNELS

It is interesting that, for all the discussions and graphs given in Sec. 6-4, there was actually no theory. No equations were solved. All of the velocity profile formulas were correlations, i.e., the results of inspired and physically meaning-

ful dimensional analysis. We can now proceed from these algebraic expressions to solve simple problems, without any extensive use of "theory." Here we discuss developed flow in ducts.

6-5.1 The Circular Pipe

Consider pipe flow first, assumed far downstream of the entrance, where velocity does not depend upon axial distance x. The laminar-flow analysis, Sec. 3-3.1, gave a parabolic velocity distribution, Eq. (3-34), plus a friction factor $C_f = 16/Re_D$, which was illustrated in Fig. 3-7. Laminar flow becomes unstable at about $Re_D = 2000$ and fully turbulent flow ensues at $Re_D \approx 4000$. At higher Reynolds numbers the data in Fig. 3-7 follow a curve labeled "Blasius," which is not a theory but a curve fit to smooth-wall data collected in 1913 by Prandtl's student H. Blasius:

$$C_f(\text{pipe}) \approx 0.0791 Re_D^{-1/4} \qquad 4000 < Re_D < 10^5 \tag{6-51}$$

The Blasius formula was one of the first modern applications of the technique of dimensional analysis. The formula is seen to have a limited range of applicability.

A better result follows from the wall law, Eq. (6-41) or (6-38a). Pipe flow, being a favorable gradient, should resemble the upper velocity profile in Fig. 6-8. Let the pipe radius be a, and let the wall coordinate be

$$y = a - r \qquad dy = -dr$$

With the profile known, we may evaluate the average pipe velocity:

$$u_{av} = \frac{Q}{A} = \frac{1}{\pi a^2}\int_0^\infty \bar{u} 2\pi r\, dr = \frac{1}{a^2}\int_0^\infty \bar{u} 2(a - y)\, dy \tag{6-52}$$

Figure 6-11 shows clearly that turbulent pipe flow has very little wake, that is, $\Pi \approx 0$. Therefore the law of the wall is accurate all the way across the pipe. Further neglect the (very thin) viscous sublayer and substitute the simple log-law, Eq. (6-38a), with the result

$$u_{av} = v^*\left(\frac{1}{\kappa}\ln\frac{av^*}{\nu} + B - \frac{3}{2\kappa}\right) \tag{6-53}$$

Now, from the definition of pipe-friction factor, $C_f = 2\tau_w/\rho u_{av}^2$, the following identities hold:

$$\frac{u_{av}}{v^*} = \left(\frac{2}{C_f}\right)^{1/2} \qquad \frac{av^*}{\nu} = Re_D\left(\frac{C_f}{8}\right)^{1/2} \qquad Re_D = \frac{2au_{av}}{\nu}$$

This piques our interest, revealing that Eq. (6-53) is actually a friction factor relation. Introducing base-10 logarithms (a tradition) plus $\kappa = 0.41$ and $B = 5.0$,

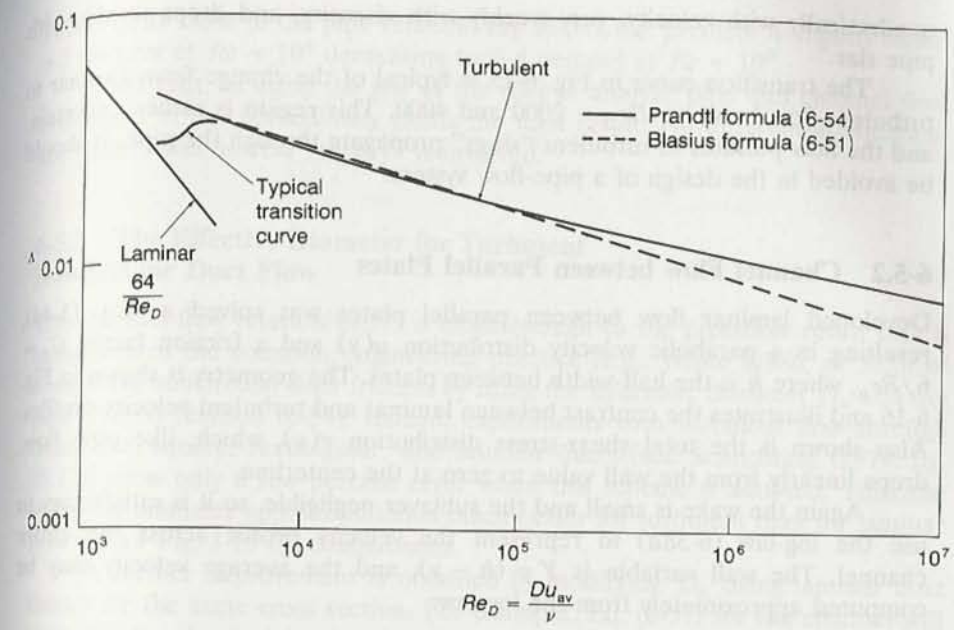

FIGURE 6-15
Analytical friction factor formulas for fully developed pipe flow. Compare with the data in Fig. 3-7.

we may clean up Eq. (6-53) as follows:

$$\frac{1}{\Lambda^{1/2}} = 1.99\log\left(Re_D\Lambda^{1/2}\right) - 1.02$$

where $\Lambda = 4C_f$ is the Darcy friction factor. This formula was derived by Prandtl in 1935. Since he neglected the sublayer and the wake, Prandtl slightly adjusted the constants to fit pipe-friction data better, especially at lower Reynolds numbers. The final formula is

$$\frac{1}{\Lambda^{1/2}} = 2.0\log\left(Re_D\Lambda^{1/2}\right) - 0.8 \tag{6-54}$$

valid for smooth-wall turbulent pipe flow for any Reynolds number greater than 4000. It supplants the Blasius correlation (6-51).

Figure 6-15 shows the laminar and turbulent friction factor formulas plotted versus Reynolds number. Note that the Blasius formula (6-51) falls too low for $Re_D > 10^5$. However, we do learn something about trends from the Blasius formula by rewriting it in terms of wall shear stress:

$$\tau_w \approx 0.0396\rho^{3/4}u_{av}^{7/4}\mu^{1/4}D^{-1/4} \tag{6-55}$$

Thus, in turbulent pipe flow, wall shear rises nearly linearly with density, nearly

quadratically with velocity, very weakly with viscosity, and drops weakly with pipe size.

The transition curve in Fig. 6-15 is typical of the change from laminar to turbulent flow between $Re_D = 2000$ and 4000. This region is rather uncertain, and the flow pulsates as turbulent "slugs" propagate through the pipe. It should be avoided in the design of a pipe-flow system.

6-5.2 Channel Flow between Parallel Plates

Developed laminar flow between parallel plates was solved as Eq. (3-44), resulting in a parabolic velocity distribution $u(y)$ and a friction factor $C_f = 6/Re_h$, where h is the half-width between plates. The geometry is shown in Fig. 6-16 and illustrates the contrast between laminar and turbulent velocity profiles. Also shown is the total shear-stress distribution $\tau(y)$, which, like pipe flow, drops linearly from the wall value to zero at the centerline.

Again the wake is small and the sublayer negligible, so it is satisfactory to use the log-law (6-38a) to represent the velocity profile across the entire channel. The wall variable is $Y = (h - y)$, and the average velocity may be computed approximately from the log-law:

$$u_{av} = \frac{1}{h}\int_0^h \bar{u}\, dY \approx v^*\left(\frac{1}{\kappa}\ln\frac{hv^*}{\nu} + B - \frac{1}{\kappa}\right)$$

Since, by definition, $u_{av}/v^* = (8/\Lambda)^{1/2}$, this is a friction factor relation. But a channel is not "round," so what is the proper Reynolds number? One obvious answer is to use the hydraulic diameter concept from Eq. (3-55):

$$Re_{D_h} = \frac{u_{av} D_h}{\nu} \qquad D_h = \frac{4A}{P} = 4h \tag{6-56}$$

Introducing this into the expression for u_{av}, using base-10 logarithms, and cleaning it all up, we obtain, for smooth-wall turbulent channel flow,

$$\frac{1}{\Lambda^{1/2}} = 2.0\log\left(Re_{D_h}\Lambda^{1/2}\right) - 1.19 \tag{6-57}$$

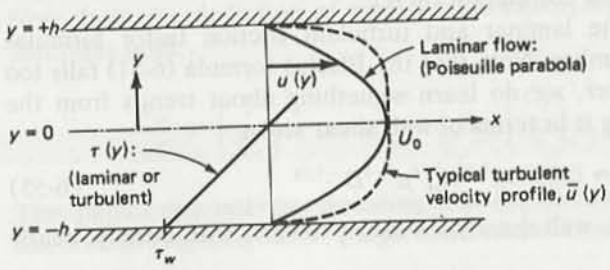

FIGURE 6-16
Fully developed laminar and turbulent flow in a channel.

This is quite close to the pipe relation, Eq. (6-54), but predicts Λ slightly higher +7 percent at $Re = 10^5$ decreasing to +4 percent at $Re = 10^8$.

Note that, in using the law of the wall to analyze pipe and channel flow, evaluation of u_{av} immediately yields the final result. No differential equations are solved, and no real "theory" is involved.

6-5.3 The Effective Diameter for Turbulent Noncircular Duct Flow

The channel-flow relation (6-57) is close enough to the pipe-flow result that it substantiates the common engineering practice [e.g., White (1986, p. 325)] of computing noncircular duct friction by using the hydraulic diameter D_h and the pipe-friction relation (6-54). Indeed, experiments with turbulent flow through triangular, square, rectangular, and annular ducts [see Schlichting (1979, fig. 20.12)] show only a few percent error when this scheme is adopted. Thus the hydraulic diameter approximation is much better for turbulent than for laminar flow (recall Fig. 3-13 for comparison).

A further improvement is obtained by modifying D_h using laminar duct theory for the same cross section. For example, Eq. (6-57) for the channel will resemble the circular pipe law (6-54) if rewritten as

$$\frac{1}{\Lambda^{1/2}}(\text{channel}) = 2.0\log_{10}\left(0.64 Re_{D_h}\Lambda^{1/2}\right) - 0.8 \tag{6-58}$$

Best agreement between channel and pipe is predicted when one uses $(0.64 D_h)$ as the *effective diameter* of the channel. Now, in laminar flow, $C_f(\text{pipe}) = 16/Re_D$, and $C_f(\text{channel}) = 24/Re_{D_h}$, and the ratio of these two is $16/24 = 0.667$, quite near the prediction of 0.64. This is no accident. A general rule for estimating turbulent friction in noncircular ducts is to use the pipe-friction law (6-54) based on an effective Reynolds number

$$Re_{D_{\text{eff}}} = \frac{u_{av} D_{\text{eff}}}{\nu} \qquad \text{where } D_{\text{eff}} = D_h \frac{16}{(C_f Re_{D_h})_{\text{laminar}}} \tag{6-59}$$

This idea was proposed and proven experimentally by O. C. Jones in tests on rectangular [Jones (1976)] and concentric annular ducts [Jones and Leung (1981)]. One could take $(C_f Re)_{\text{laminar}}$ for the given section from the results in Sec. 3-3.3. The method should work well for any squatty or blocky cross section, i.e., with no unusually thin regions. An experiment by Eckert and Irvine (1957) on a 12° isoceles triangle gave poorer results, because the flow in the 12° corner remained laminar up to surprisingly high Reynolds numbers. Obot (1988) reviews the entire subject of noncircular ducts, including small apex angles and rough walls. While agreeing with the effective diameter scheme, Obot goes further and proposes a "critical friction" or transition-oriented method for correlating the data in any duct.